PERGAMON

International Journal of Solids and Structures 38 (2001) 4091–4117

INTERNATIONAL JOURNAL OF SOLIDS and STRUCTURES

www.elsevier.com/locate/ijsolstr

Influence of nonlinearity and double elasticity on flexure of rock beams — I. Technical theory

G.E. Exadaktylos [a,*], I. Vardoulakis [b], S.K. Kourkoulis [b]

[a] *Rock Mechanics Laboratory, Department of Mineral Resources Engineering, Technical University of Crete, GR-73100 Chania, Greece*
[b] *Department of Engineering Science, Section of Mechanics, National Technical University of Athens, 5 Heroes of Polytechnion Avenue, Zografou Campus, GR-15773 Athens, Greece*

Received 28 January 1999

Abstract

As a rule, solids display nonlinearity during loading in the relation between strains and stresses. Deviations from Hooke's linear constitutive law were also registered in the range of initial, small loads both in uniaxial compression and tension of crystalline rocks. Nonlinearity of strain in rocks is manifested primarily in the stress dependency of tangent or secant elasticity modulus and Poisson's ratio and is caused by closure, initiation, propagation and linkup of pre-existing and new microcracks, frictional sliding along cracks, growth of dislocations, etc. Many experimenters and standardization procedures assume that the dependence of the strain on the applied stress is linear and for practical calculations only two elasticity constants are used: the tangent or secant elasticity modulus at 50% of the failure load in compression and Poisson's ratio at the same stress level. Apart from nonlinearity many rock types and concretes have quite different stress–strain relations in tension and compression. Yet direct tensile testing is seldom performed because of its many inherent difficulties. Such unrecognized double elasticity and nonlinearity of rocks can invalidate a stress analysis, and in addition, produce a meaningless overestimate (or underestimate) of tensile strength based upon the modulus of rupture derived from a bending test. In Part I of the present study, it is shown that both double elasticity and nonlinearity have a profound effect on flexural strength of rocks as predicted by application of fundamental continuum damage mechanics relations and an appropriate technical theory. The proposed theory is validated in Part II of this work, in which an appropriate back-analysis procedure is suggested for the characterization of the mechanical properties of Dionysos marble in the uniaxial tension and compression regime from properly designed three-point bending tests.

Keywords: Nonlinearity; Elasticity; Rock beams; Theory

1. Introduction

The tensile strength of rock is generally stated to be less than approximately 10% of its compressive strength. Griffith's theory predicts that the uniaxial compressive strength of rocks is eight times the uniaxial

* Corresponding author. Address: 8 Lamias str., GR-11523 Ambelokipi, Athens, Greece. Fax: +30-1-699-4116.
E-mail address: exadakty@mred.tuc.gr (G.E. Exadaktylos).

0020-7683/01/$ - see front matter
PII: S0020-7683(00)00251-1

tensile strength, whereas Murrell's extension of the Griffith criterion gives the value of ratio of compressive strength over tensile strength equal to twelve (Jaeger and Cook, 1976). Hence, the experimental determination of tensile strength of rocks is of great importance in current rock engineering practice regarding prevention of rock failure of underground and superficial works, as well as in structural engineering practice in which the characterization and residual life prediction of natural building stones used in monuments and buildings is of overwhelming importance. Despite the importance of the tensile strength of rock in practice and in connection with theories of failure, direct measurements of tensile strength are difficult and are not commonly conducted in rock mechanics laboratories. This is because both the bending stresses or torsion moment (inevitably caused by the eccentricity of machine axial loads) and the anomalous concentrated stresses (included by an improper connection during testing between the ends of a rock specimen and the machine caps serving to transfer the tensile loads to the specimen) are frequently unavoidable (Barla and Goffi, 1974; Nova and Zaninetti, 1990). Thus, it has sometimes been common practice to neglect tensile properties or replace tensile properties by compressive properties as an input parameter in the engineering analysis.

Indirect tests such as beam flexure and diametral compression of discs or annuli have the inherent disadvantage that a stress–strain relationship must be assumed in order to obtain usable results; the usual assumption of linear elasticity, with equal moduli in compression and tension, is invalid for many rocks (Wuerker, 1955; Blair, 1956). Bimodularity or bilinearity of rocks is important in the disc and bending tests, as well as in the case of underground excavations such as tunnels or other regular and irregular openings in which tensile stresses may occur.

Long before the above investigators it has been known that certain materials behave significantly differently in tension than in compression. For example, this was recognized by Saint-Venant (1864), who analyzed the pure bending behavior of a beam having different non-linear stress–strain curves in tension and compression. Specific experimental evidence of bimodularity has been reported for cast iron by Gilbert (1961), cord-rubber by Clark (1963), polymers by Zemlyakov (1965), concrete by Seefried et al. (1967), cortical bone by Simkin and Robin (1973), soft biological tissue by Pearsall and Roberts (1978), and various kinds of rock by Haimson and Tharp (1974). Of course, the specific micromechanisms responsible for double elasticity vary from one class of material to another; stiff and brittle solids such as rocks, concrete and ceramics exhibit simultaneous microcrack closure and sliding along microcracks and even local tensile cracking from tips of fissures at low stress levels in compression, whereas only crack extension occurs in tension; on the other hand, soft fiber-reinforced materials are weakened in compression by fiber microbuckling. Haimson and Tharp (1974) have presented linearized uniaxial compression and tension data indicating that the slope of the line in compression is almost always higher than that in tension. This ratio of slope in tension to that in compression can in fact vary from 1:1 in very tight rocks, to 1:2 in some limestones, to 1:20 in weak sandstones, to 0 in no-tension fractured rocks or soils. However, the linearization of the uniaxial compression curve masks the nonlinearity of rocks at low stress where tangent modulus increases as the stress increases. Eventually, in uniaxial compression, a stress is reached after which the curve becomes quasi-linear but the tangent modulus at this stress level is much higher than that at low stress levels (Walsh, 1965). Thus, deviations from Hooke's law which are also registered in the range of initial, small loads in compression must be considered in the interpretation of indirect tension tests involving both extensional and compressive stresses (i.e., bending and disc tests). Irregularity of the stress–strain behavior of rocks has not been studied so thoroughly in the past, and it is frequently assumed that the dependence of their strain on the applied stress is close to linear, whereas for practical calculations only two elasticity constants are used, namely the elasticity modulus and Poisson's ratio (both constants are usually defined at 50% of the failure load). Further, load-carrying capacity evaluation based on linear elasticity and on a maximum extension strain criterion is usually overestimated.

The values of the tensile strength determined from bending tests on rock are often significantly greater than the tensile strength measured from direct tension tests. It is remarked here that there exist cases where

the rock tensile strength measured from a bending test may be lower than the respective strength determined from a uniaxial tensile test. Although this effect was not understood, it was well recognized, and the term "modulus of rupture" is used for the extreme tensile stress determined from a bending test. Fairhurst (1961) discussed the effects of different values for Young's modulus in tension and compression on bending tests and describes apparatus for four-point bending (4PB) tests. He proposed an indirect methodology for the estimation of tensile modulus from load-deflection measurements in 4PB and from measurement of compressive modulus in uniaxial compression. Later Adler (1970), by using the "transformed section" concept of mechanics of materials, extended Fairhurst's analysis, which was restricted to prismatic specimens, to employ flexural test results on cylindrical specimens (i.e., drill cores) in determining the tensile tangent modulus of elasticity and the correct modulus of rupture of bilinear rock materials. However, in the 4PB loading configuration the bending moment, the tensile stress and the bending curvature remain constant in the region between the points of load application. Hence, the crack can start anywhere between these points. In such a case if the determination of the post-peak behavior of rock is of interest, the use of unnotched beams may not be the best choice due to this inherent experimental difficulty (i.e., the a priori unknown position of crack initiation). For example, the use of crack mouth opening displacement control requires long connecting rods. On the other hand, if a notched beam approach is employed then a larger number of specimens is required and the analysis of notch effect should be carried out.

Alternatively, in three-point bending (3PB) test both the bending moment and the tensile stress reach maximum value immediately beneath the point of load application and consequently the crack starts always at specimen mid-span (note that this statement may not be valid for disordered or inhomogeneous materials). However, near the point of application of the concentrated load a serious local perturbation in stress–strain distribution should be expected, and a further investigation of the problem is necessary. Herein, the classical Bernoulli–Euler technical bending theory is further elaborated by considering the double elasticity (bilinearity) and nonlinearity due to damage in the tensile regime of crystalline rocks. The methodology that is used for this development is based on classical analyses followed in the past by Bach and Baumann (1914), Nadai (1950), Timoshenko (1956) and Marin (1962). The theory applies equally well for both 4PB and 3PB bending configurations provided that *Saint-Venanit's* principle is satisfied, that is the regions under consideration are at a considerable distance from any place of loading or of support. If strain measurements are conducted in such places at upper and lower outermost fibers of the beam then the proposed theory permits one to evaluate the double elasticity of rocks. However, in many cases, such as for example the 3PB test, we are interested in the state of affairs near to the place of concentrated load, since at that region the crack starts to propagate. For this purpose, it is demonstrated numerically by employing an indirect boundary element model that both axial (or longitudinal) and transverse principal stresses reach very high values in a skin adjacent to the concentrated loading place. It is shown that Stokes' empirical formula for the correction of horizontal stresses at beam mid-section as was further corrected by Seewald (Timoshenko and Goodier, 1970) is in error close to the lower edge of the beam. It is further illustrated that the nonlinearity of stress–strain relation in uniaxial tension of the material produces a nonlinear distribution of bending curvature along the axis of the beam. If this bending curvature nonlinearity is measured during a 3PB bending test then the damage modulus of the material in uniaxial tension may be deduced in the framework of an inverse procedure. Further, it is demonstrated that neglecting the bimodularity and nonlinearity of the tensile behavior of britttle rocks may lead to significant overestimation of the load-carrying capacity of rock beams and of uniaxial tensile strength which in turn severely affect design validity.

The proposed theory is validated in Part II (Exadaktylos et al., 2000) based on 3PB bending experimental data of the well known Dionysos marble that is used for restoration of Acropolis of Athens (Korres, 1993; Zambas, 1994) and it is demonstrated that it constitutes a rational attempt in establishing a simple, engineering analytical tool quantifying processes occurring in rocks which are subjected to tensile stresses. It is based on a sound engineering strategy, i.e., to start from simple relations, establish the simplest

meaningful theory and test it against experimental data in order to prove whether it can be used for the material in question.

2. Theory of stress–strain properties in bending

2.1. Basic equations of technical bending theory

Herein, for easy reference, the classical engineering theory of beam bending will be outlined briefly. To fix ideas we consider a simply supported beam of rectangular cross-section under the action of a vertical load P at its upper surface and at the mid-span. The longitudinal section of the beam is referred to a Cartesian coordinate system O(x,y,z) positioned on the neutral axis with its origin at mid-span and with the Ox axis directed along the neutral axis of the beam and the Oz axis extending vertically downwards as it is illustrated in Fig. 1a. Further, deformation quantities are assumed as infinitesimal, and the corresponding displacements of points in a cross-section in x and z directions are denoted by the symbols u, w, respectively, as it is shown in Fig. 1a.

The kinematic quantities of the axial strains ε_{xx}, ε_{zz} and the engineering shear strain γ_{xz}, respectively, are defined as usual

$$\varepsilon_{xx} = u_{,x}\,, \qquad \varepsilon_{zz} = w_{,z}\,, \qquad \gamma_{xz} = u_{,z} + w_{,x}\,, \tag{1}$$

where partial differentiation with respect to a coordinate x, z has been indicated by an additional subscript x or z preceded by a comma. The horizontal displacement u along x direction at a given normal section of the beam, is set linear, i.e.,

$$u = \psi(x)z, \tag{2}$$

where, as it is shown in Fig. 1b, the symbol ψ denotes the rotation of the normal cross-section. In view of relationship (2), plane sections are assumed to remain plane. In Fig. 1a z_c, z_t, are positive numbers denoting respectively the compressive and tensile outer fiber distances, H is the thickness (depth) of the beam, B denotes the width of the beam, and the symbols σ_{xx}, τ_{xz} denote the axial and shear stresses, respectively. Further, the second moment of area of the cross-section of the beam is defined as follows:

$$I = \frac{BH^3}{12}. \tag{3}$$

By setting the bending curvature of the beam as follows:

$$\kappa \equiv \psi_{,x}\,, \tag{4}$$

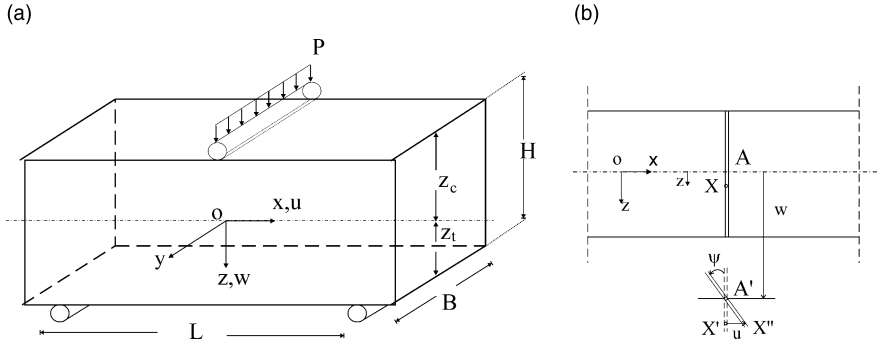

Fig. 1. (a) The geometry of the beam in 3PB and the coordinate system, and (b) components of the displacement (u, w) and deformation ψ.

then from relationships (1), (2) and (5), the axial (longitudinal) component of the strain can be written as follows:

$$\varepsilon_{xx} = \kappa z. \tag{5}$$

2.2. Nonlinearity at small and large strains of brittle rocks

The beam material may have arbitrary uniaxial stress–strain behavior in the longitudinal directions, i.e., the mechanical behavior of the material in uniaxial loading is represented by a law of the form:

$$\sigma = \begin{cases} \sigma_t(\varepsilon) & \text{for tension,} \\ \sigma_c(\varepsilon) & \text{for compression,} \\ \sigma_t(0) = \sigma_c(0) = 0, \end{cases} \tag{6}$$

where we have set $\sigma \equiv \sigma_{xx}$, $\varepsilon \equiv \varepsilon_{xx}$ and $\sigma_t(\varepsilon), \sigma_c(\varepsilon)$ are continuous functions referring to uniaxial tension and uniaxial compression, respectively. Here, the following polynomial relationship is proposed to approximate the stress–strain behavior of a variety of rock types:

$$\sigma = \begin{cases} \sigma_t(\varepsilon) = E_t\varepsilon + F_t\varepsilon^2 & \text{for tension,} \\ \sigma_c(\varepsilon) = E_c\varepsilon + b\varepsilon^2 + c\varepsilon^3 & \text{for compression,} \end{cases} \tag{7}$$

with E_t, E_c denoting the *initial tangent moduli* in tension and compression, respectively, and F_t, b, c being additional material constants. Thereafter, all strains are taken to be positive numbers unless otherwise stated. The uniaxial stress–strain relations (6) or (7) are used directly in beam theory by neglecting Poisson-type lateral contraction effects.

It is worth noting that the detailed analysis carried out by Bell (1984) showed that the first who proposed the nonlinear (parabolic) law given by the first of relations (7) (with $F_t < 0$) based on direct tension tests on steel piano wire was Gerstner, Franz Joseph, in 1824. The results of Gerstner's tests and the nonlinear law were published in 1831 in the third chapter of the first volume of his *Handbuch der Mechanik*. It can be shown that this uniaxial tension constitutive law can be derived from a simple probabilistic theory for brittle materials. In such a theory, the stress and strain variables are considered to be random variables. The random stress is denoted by s whereas the probability density of stress is denoted by $f(s)$. Then, the nominal stress is the expected mean stress, in the probabilistic sense, defined as follows:

$$\sigma_t = \int_{-\infty}^{\infty} sf(s)\,\mathrm{d}s = \overline{\sigma}(1 - D), \tag{8}$$

where $\overline{\sigma}$ is the expected value of the nominal stress in the uncracked region (actual stress) that is related to the strain by a linear law:

$$\overline{\sigma} = E_t\varepsilon. \tag{9}$$

In Eq. (15), D is the "damage factor" or "decohesion probability", defined as

$$D = \frac{A - \overline{A}}{A}, \tag{10}$$

with A denoting the initial cross-sectional area of the specimen and $\overline{A}$ denoting the effective (undamaged) load transmitting area of the cross-section; thus, $A - \overline{A}$ is the total area occupied by fissures and micro-cracks. Prior to formation of the first cracks $A = \overline{A}$ and consequently $D = 0$. In the other limiting case the working area $\overline{A}$ can become zero giving $D = 1$, i.e., $0 \leqslant D \leqslant 1$. In a generalization of *Saint-Venant* strength theory, D depends on strain and in a first approximation it can be taken to be proportional to the strain ε, namely

$$D = -\frac{F_t \varepsilon}{E_t} + \mathrm{O}(\varepsilon^2), \tag{11}$$

in which O denotes the Landau order-of-magnitude symbol and $F_t \leqslant 0$ in order D to be positive. From Eqs. (8), (9) and (11) the parabolic law represented by the first of relations (7) can be deduced. Fig. 2 below illustrates graphically the first of constitutive equations (7) in direct tension and the damage evolution law (11).

On the other hand, the most obvious departure from ideal linear elastic behavior to be shown by the uniaxial compression test is nonlinearity of the stress–strain characteristic both in the beginning of the test and close to the peak load. The first part of a typical plot of stress against strain for a high-strength crystalline rock curves so as to increase the slope with increasing stress (Fig. 3, stage I). This curvature gradually ceases, until at the mid-portion of the plot there is approximate linear proportionality between stress and strain (Fig. 3, stage II). The initial curvature in Stage I for $0 \leqslant \sigma \leqslant \sigma_r$, that is described by the parabolic relationship $\sigma_c(\varepsilon) \approx E_c\varepsilon + b\varepsilon^2,\ b > 0$, implies 'stiffening' of the rock with increasing stress and is attributed to the predominant mechanism of progressive closure of cracks and pores under stress. For $\sigma = \sigma_r$ the surfaces delimiting microcracks appear to be closed and the value of the tangent elastic modulus stabilizes in the value of E_{50} that is also the tangent modulus at 50% of the ultimate stress. This effect has been analyzed in some detail by Brace (1965), Walsh (1965), and Walsh and Brace (1966). The linear relation of stage II is taken to represent elastic straining of the constituent grains after pore closure has reached a limit for the particular stress system. In soft rocks, the initial curvature of stage I is not always measurable. At stresses approaching the uniaxial compressive strength of the rock, the slope of the stress–strain curve decreases (Fig. 3, stage III). This effect, which also marks the onset of dilation, is associated with formation of microcracks, which progressively destroy the loading-bearing capacity of the rock and permit irreversible strain (permanent set) to occur, and is described by the second of relations (7) with $c < 0$. The uniaxial compression test in a non-stiff configuration culminates when the slope of the stress–strain curve approaches zero and the unconfined compressive strength of the rock σ_{cu} is reached.

The cubic law in uniaxial compression represented by the second of constitutive relationships (7) may be easily derived by postulating that the decohesion probability is dependent on the strain by a parabolic relation, i.e.,

$$D = -\frac{1}{E_c}\left(b\varepsilon + c\varepsilon^2\right) + \mathrm{O}(\varepsilon^3), \qquad \overline{\sigma} = E_c\varepsilon. \tag{12}$$

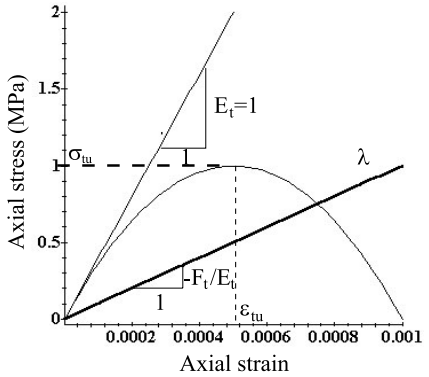

Fig. 2. Linear versus nonlinear behavior of rock in uniaxial tension regime. The plot of the linear damage law (11) is also graphically displayed. E_t denotes the initial tangent elasticity modulus, whereas σ_{tu}, ε_{tu} denote the strength and extension strain at peak stress, respectively, of rock in uniaxial tension.

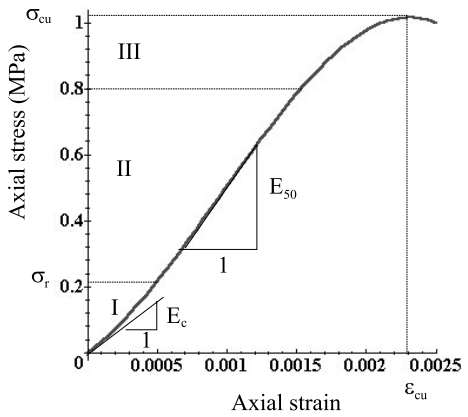

Fig. 3. Typical nonlinear axial stress–strain diagram of a rock in uniaxial compression.

By solving the second of relations (7) with respect to ε for the case of $c = 0$, we derive

$$\varepsilon = \hat{\sigma}[1 - \hat{b}\hat{\sigma} + 2\hat{b}^2\hat{\sigma}^2] + \mathrm{O}(\hat{\sigma}^4), \qquad \hat{\sigma} = \frac{\sigma}{E_c}, \qquad \hat{b} = \frac{b}{E_c}. \tag{13}$$

The polynomial relation (13) is known as Hartig's law, proposed in 1893, on the basis of tensile tests on leather, rubber, metals and clay (Hartig, 1893). Deformation of the type (13) is characterized by the following relationship of the tangent stiffness with respect to stress:

$$E = \frac{\mathrm{d}\sigma}{d\varepsilon} \approx E_c[1 + 2\hat{b}\hat{\sigma}] + \mathrm{O}(\hat{\sigma}^2), \quad E_c \leqslant E \leqslant E_{50}. \tag{14}$$

Experimental evidence indicates that for many rocks $E_t \leqslant E_{50}$, with the moduli ratio E_t/E_{50} varying from 1:1 for very coherent rocks to 1:2 for some limestones, to 1:20 in weak sandstones, to 0 in no-tension materials (e.g. soils or heavily discontinuous rocks) (Table 1). Hence, with the complete deformation spectrum, rock stress–strain relationship can be at best simplified into a bilinear curve with point of

Table 1
Tangent elastic moduli in tension and compression (Haimson and Tharp, 1974)

Rock type	E_t (GPa)	E_{50} (GPa)	E_{50}/E_t	E_t/E_{50}
Westerly granite	17.2	72.4	4.21	0.24
Austin limestone	11.7	15.8	1.35	0.74
Carthage limestone	35.2	63.4	1.80	0.55
Indiana limestone	11.0	26.9	2.45	0.41
Georgia marble	23.4	42.1	1.79	0.56
Tennessee marble	53.1	76.5	1.44	0.69
Russian marble	9.0	20.7	2.30	0.43
Star mine quartzite	75.8	75.8	1.00	1.00
Arizona sandstone	11.7	45.5	3.88	0.26
Berea sandstone	4.1	23.4	5.70	0.18
Millsap sandstone	0.7	13.1	18.71	0.05
Tennessee sandstone	1.4	16.5	11.79	0.08
Russian sandstone	11.7	57.2	4.88	0.21

intersection at zero stress and in general the rock is regarded as a ''bimodulus'' material. The assumption of *bilinearity* can and should be incorporated in the analytical approach to any problem that involves mixed stresses at a point. On the other hand, one cannot exclude cases of particular interest in bending of rock beams where the rock material exhibits a special anisotropy of the form $E_c < E_t$.

The above proposed constitutive relationships (7) for rocks can be considered as a generalization of Krajcinovic's (1979) model for plain concrete. In this case,

$$E_c = E_t = E, \qquad F_t = -\frac{E^2}{D_t}, \qquad b = c = 0 \tag{15}$$

with D_t denoting the tensile-microcrack-damage modulus ($D_t > 0$) related to Janson and Hult (1977) linear version of Kachanov (1958) concept of continuum damage mechanics (Bert, 1983). Moreover, the proposed model in compression expressed by the second of relations (7) is a generalization of Bert's model (1983) that is stated as follows:

$$\sigma_c(\varepsilon) = E_c\varepsilon + F_c\varepsilon^2, \quad F_c \leqslant 0. \tag{16}$$

The above simple model (16) can be used in a large class of rocks that do not exhibit significant crack closure in the initial state of unconfined compression loading (that is, stage I is missing).

The strains at which tensile and compression instability occurs can be computed by applying the following instability criterion first proposed by Gerstner in 1832 (Bell, 1984):

$$\frac{d\sigma_i}{d\varepsilon} = 0, \quad i = t, c. \tag{17}$$

By combining relations (7) and (17), it is derived

$$\varepsilon_{tu} = -\frac{E_t}{2F_t},$$
$$\varepsilon_{cu} = \begin{cases} -\frac{E_c}{2c}, & b = 0, \\ -\frac{\sqrt{b^2-3cE_c}-b}{3c}, & b \neq 0, \end{cases} \tag{18}$$

where ε_{tu}, ε_{cu} are the ultimate strains at which instability occurs in direct tension and unconfined compression, respectively. Note that since both damage parameters are negative quantities then ε_{tu}, ε_{cu} are positive quantities (i.e., in accordance to the sign convention employed herein). If the first of relations (18) is combined with Eq. (11), then the following value of decohesion probability (or damage factor) $D_f = D$ at $\varepsilon = \varepsilon_{tu}$ is found at fracture of a rock specimen under direct tension:

$$D_f = \tfrac{1}{2}, \tag{19}$$

whereas according to Eq. (10), the effective area $\overline{A}$ of the cross-section at fracture is reduced to one-half of the original. Also, in view of relationships (7) and (18), the predicted tensile and compressive strengths may be found in the following manner:

$$\sigma_{tu} = -\frac{E_t^2}{4F_t},$$
$$\sigma_{cu} = \begin{cases} -\frac{E_c^2}{4c}, & b = 0, \\ \frac{\left(\sqrt{b^2-3cE_c}+b\right)\left(-6cE_c+b^2+b\sqrt{b^2-3cE_c}\right)}{27c^2}, & b \neq 0\,. \end{cases} \tag{20}$$

in which σ_{tu}, σ_{cu} denote the ultimate stress in direct tension and unconfined compression, respectively. Due to the fact that at stress levels as low as those causing rupture in tension or brittle polycrystalline materials

(e.g. rocks, ceramics, concrete, etc.), the compressive stresses are not sufficient to cause dilation of rock, then for most practical purposes the constant c entering the second of constitutive relations (17) may be discarded in subsequent calculations of beam bending theory, i.e. $c \approx 0$.

2.3. Bending of nonlinear materials with different behavior in tension and compression

Next, following the classical method of analysis (Nadai, 1950; Timoshenko, 1956; Marin, 1962) the longitudinal strains for the outer fibers of the beam are obtained from relation (5) as follows:

$$\varepsilon_t = \kappa z_t, \qquad \varepsilon_c = \kappa z_c, \qquad \frac{\varepsilon_t}{\varepsilon_c} = \frac{z_t}{z_c}, \tag{21}$$

where ε_t represents a tensile strain, and ε_c, a compressive one. The strains defined by these relations would be known if the position of the neutral axis and the bending curvature were known. The kinematic quantities can be found from the following equilibrium equations of forces in the axial direction and moments:

$$\begin{aligned} &\int_{-\hat{z}_c}^{0} \sigma_c(\hat{\kappa}\hat{z})\,\mathrm{d}\hat{z} + \int_{0}^{\hat{z}_t} \sigma_t(\hat{\kappa}\hat{z})\,\mathrm{d}\hat{z} = 0, \\ &\int_{-\hat{z}_c}^{0} \hat{z}\sigma_c(\hat{\kappa}\hat{z})\,\mathrm{d}\hat{z} + \int_{0}^{\hat{z}_t} \hat{z}\sigma_t(\hat{\kappa}\hat{z})\,\mathrm{d}\hat{z} = \frac{M}{BH^2} \end{aligned} \tag{22}$$

where it is assumed that the material is subjected to a bending moment M, whereas there is no applied axial tension or compression. The following dimensionless variables were employed in relations (22):

$$\hat{z} = \frac{z}{H}, \qquad \hat{z}_t = \frac{z_t}{H}, \qquad \hat{z}_c = \frac{z_c}{H}, \qquad \hat{\kappa} = \kappa H. \tag{23}$$

Since $\hat{z} = \hat{\kappa}^{-1}\varepsilon$ and $\mathrm{d}\hat{z} = \hat{\kappa}^{-1}\,\mathrm{d}\varepsilon$, then from the first term of relationship (22), it is obtained

$$\int_0^{\varepsilon_c} \sigma_c(\varepsilon)\,\mathrm{d}\varepsilon = \int_0^{\varepsilon_t} \sigma_t(\varepsilon)\,\mathrm{d}\varepsilon \iff \int_{-\varepsilon_c}^{\varepsilon_t} \sigma(\varepsilon)\,\mathrm{d}\varepsilon = 0, \tag{24}$$

which means than in order to determine the neutral axis of the beam, the total strain $\Delta = \varepsilon_t + \varepsilon_c$ must be selected so that the areas enclosed by the σ–ε curve and the axis of strains to be equal. Then, substituting Eq. (7) into Eq. (24) and solving for the compressive strain, it is obtained

$$\varepsilon_c = \begin{cases} \dfrac{\sqrt{m(3+2m_f\varepsilon_t)}\varepsilon_t}{\sqrt{3}m}, & b = 0, \\ \dfrac{m^2+e_1^2-me_1}{2m_b e_1}, & b \neq 0 \end{cases} \tag{25}$$

in which

$$\begin{aligned} &m = \frac{E_c}{E_t}, \qquad m_f = \frac{F_t}{E_t}, \qquad m_b = \frac{b}{E_t}, \\ &e_1 = (4m_b^2 m_f \varepsilon_t^3 + 6m_b^2\varepsilon_t^2 - m^3 + 2m_b\varepsilon_t(4m_b^2 m_f^2\varepsilon_t^4 + 12m_b^2 m_f\varepsilon_t^3 + 9m_b^2\varepsilon_t^2 - 2m^3 - 2m_f m^3\varepsilon_t)^{1/2})^{1/3}. \end{aligned} \tag{26}$$

The asymptotic expansion of the compression strain around infinitesimal tensile strains for $b = 0$ has the much simpler form

$$\varepsilon_c \approx \frac{1}{\sqrt{m}}\varepsilon_t + \frac{1}{3}\frac{m_f}{\sqrt{m}}\varepsilon_t^2 + \mathrm{O}(\varepsilon_t^3). \tag{27}$$

Formula (27) may be employed for the experimental evaluation of the parameters m and m_f by curve fitting ε_c–ε_t data from a bending test performed on a low-porosity rock (Exadaktylos et al., 2000).

Further, from the third term of Eq. (21) and relation (25), as well as from the necessary geometric relationship $z_c + z_t = H$, we find the relation

$$\hat{z}_t = \begin{cases} \frac{m}{m+\sqrt{m(1+\frac{2}{3}m_f\varepsilon_t)}}, & b = 0, \\ \frac{1}{1+\frac{m(m-e_1)+e_1^2}{2m_b e_1 \varepsilon_t}}, & b \neq 0. \end{cases} \tag{28}$$

The series expansion of the first term of the above expression (28) around small extension strains is

$$\hat{z}_t \approx \frac{m}{m+\sqrt{m}} - \frac{1}{3}\frac{m^{3/2}}{(m+\sqrt{m})^2} m_f \varepsilon_t + \frac{1}{18} m^2 \frac{(3+\sqrt{m})}{(m+\sqrt{m})^3} (m_f \varepsilon_t)^2 + \mathrm{O}\Big((m_f \varepsilon_t)^3\Big). \tag{29}$$

It can be easily verified from this formula that in the case of $m_f = b = 0,\ m = 1$, then $\hat{z}_t = 0.5$, that is to say, the neutral axis passes through the centroid of the cross-section. Curves showing the variation of $\hat{z}_t$ with outer fiber extension strain ε_t for various values of the modulus ratio m are shown in Fig. 4. It may be seen from the figure that the neutral line of the beam that exhibits damage shifts during the increase of strain to the concave side of the beam, thus increasing the region where tensile forces act with this increase to be more pronounced as the modulus ratio increases.

The constitutive relation of M is derived by substituting $\hat{z} = \hat{\kappa}^{-1}\varepsilon$ and $\mathrm{d}\hat{z} = \hat{\kappa}^{-1}\,\mathrm{d}\varepsilon$ into the second term of Eq. (22):

$$\int_{-\varepsilon_c}^{\varepsilon_t} \sigma\varepsilon\,\mathrm{d}\varepsilon = \frac{M}{BH^2}\hat{\kappa}^2. \tag{30}$$

From the above equation, the constitutive relationship of the bending moment may be deduced

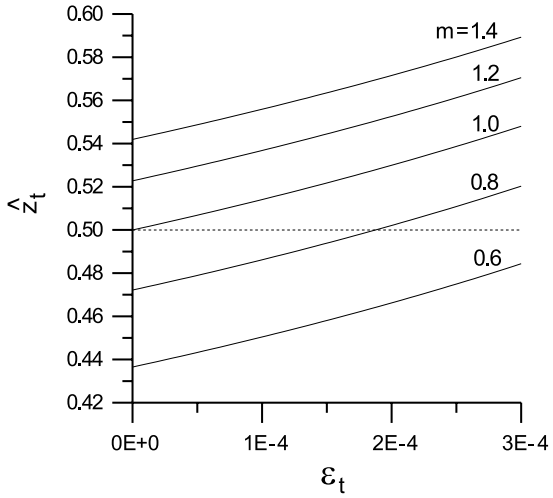

Fig. 4. Graphical representation of the dimensionless tensile outer fiber distance $\hat{z}_t$ with maximum tensile strain ε_t for five values of the modulus ratio $m = E_c/E_t$ at hand and for $m_f = -1600$, $m_b = 0$.

$$M = E_r I\kappa, \qquad E_r = \frac{12}{\hat{\kappa}^3}\int_{-\varepsilon_c}^{\varepsilon_t} \sigma\varepsilon \,\mathrm{d}\varepsilon, \tag{31}$$

where the symbol E_r designates the reduced modulus of the beam. The closed form expression for the reduced elastic modulus can be found from the second term of Eq. (31) and relationship (7) as follows:

$$\hat{E}_r = \frac{E_r}{E_t} = \begin{cases} \dfrac{3m\{4\sqrt{3}\sqrt{[m(2m_f\varepsilon_t+3)]^3}+36m^2+27m_f m^2\varepsilon_t\}}{\{\sqrt{3}\sqrt{m(2m_f\varepsilon_t+3)}+3m\}^3}, & b=0, \\ \dfrac{3m_f\varepsilon_t^4+4\varepsilon_t^3+(m/2)n^3+(12/64)m_b n^4}{((1/2)n+\varepsilon_t)^3}, & b\neq 0, \end{cases} \tag{32}$$

where we have put

$$n = \frac{m^2+e_1^2-me_1}{m_b e_1}. \tag{33}$$

Obviously for $\sigma = E\varepsilon$ and $\varepsilon_c = \varepsilon_t$, we get $E_r = E$. The following asymptotic value of the dimensionless reduced modulus $\hat{E}_r$ corresponding to the linearized uniaxial compression model (b = 0) can be also derived:

$$\hat{E}_r \approx \frac{4m}{(1+\sqrt{m})^2} + \frac{3m^3}{(\sqrt{m}+m)^3}(m_f\varepsilon_t) - \frac{5}{3}\frac{m^4(\sqrt{m}+1)}{(\sqrt{m}+m)^5}(m_f\varepsilon_t)^2 + \mathrm{O}\Big((m_f\varepsilon_t)^3\Big), \quad m_b = 0. \tag{34}$$

It is rather obvious that for the case $m_f = 0$ the above formula takes the simple form given by Timoshenko (1956),

$$\hat{E}_r = \frac{4m}{(1+\sqrt{m})^2}, \qquad m_f \to 0, \qquad m_b = 0. \tag{35}$$

As it is noted by Timoshenko (1956), the above modulus is sometimes used in calculating the buckling load of a column compressed beyond the proportionality limit of the material. The first who proposed this formula was Engesser (1895). The dependence of reduced modulus on the extension strain at outer fiber is illustrated in Fig. 5 for five values of the modulus ratio at hand and for a damage parameter $m_f = -1600$.

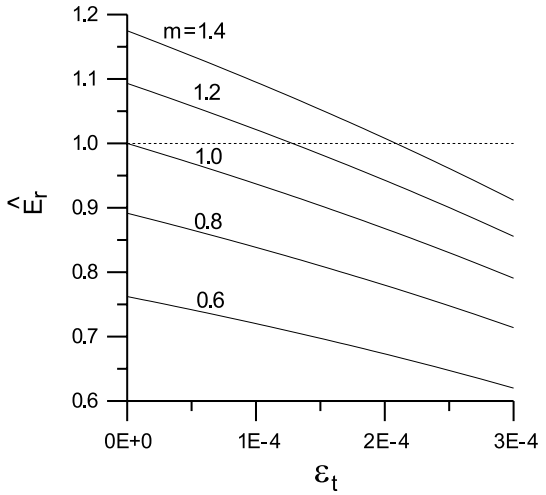

Fig. 5. Dependence of the dimensionless reduced modulus $\hat{E}_r$ on the tensile outer fiber strain ε_t for five values of the relative modulus ratio at hand and for $m_f = -1600$, $m_b = 0$.

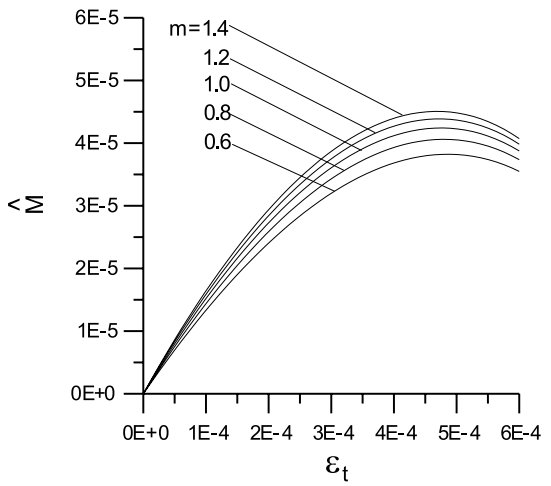

Fig. 6. Relation between dimensionless bending moment $\hat{M}$ and tensile outer fiber strain ε_t for various values of the tangent modulus ratio m and for $m_f = -1600$, $m_b = 0$.

As it was intuitively expected the modulus of elasticity of the beam decreases as the strain and consequently the damage of the beam increases.

Thereafter, by recourse to relationships (31) and (32), the following formula is obtained for the bending moment:

$$\hat{M} = \frac{M}{E_t H^2 B} = \frac{1}{12} \frac{\left\{ 4\sqrt{3}\sqrt{[m(2m_f\varepsilon_t + 3)]^3} + 36m^2 + 27m_f m^2 \varepsilon_t \right\} \varepsilon_t}{\{\sqrt{3}\sqrt{m(2m_f\varepsilon_t + 3)} + 3m\}^2}, \quad b = 0. \tag{36}$$

The asymptotic expansion for the normalized bending moment around small values of ε_t reads as follows:

$$\hat{M} \approx \frac{(m^{3/2} + m^2)}{3(\sqrt{m} + m)^2} \varepsilon_t + \left[\frac{1}{4} \frac{(4m^{3/2} + 3m^2)}{(\sqrt{m} + m)^2} - \frac{2}{9} \frac{(m^{3/2} + m^2)\sqrt{m}}{(\sqrt{m} + m)^3} \right] m_f \varepsilon_t^2 + O(\varepsilon_t^3). \tag{37}$$

The dependence of bending moment on outermost extension strain for various values of the modulus ratio m and for $m_f = -1600$, $m_b = 0$ is illustrated in Fig. 6.

It is of importance to determine also the bending moment and the extension strain for which the bottom fiber ceases to support tensile stresses. As it has been proposed by Bert (1983), as well as Bert and Kumar (1980) the critical tensile strain for bending instability, ε_{bu} can be found by applying to relation (36) the following instability criterion:

$$\frac{d\hat{M}}{d\varepsilon_t} = 0. \tag{38}$$

For the specific case of $m = 1$, it may be shown that

$$\varepsilon_{bu} = -\tfrac{4}{5} m_f^{-1}, \quad b = 0. \tag{39}$$

The above value of the critical tensile strain should be compared with that given by the first term of relation (18) depicting the failure tensile strain in direct tension. This comparison reveals that the critical

strain for bending rupture that is calculated by the bending failure criterion is 1.6 times the critical tensile strain calculated by Gerstner's uniaxial stress instability criterion (17). In the more general case of a bimodulus rock, the following asymptotic relationship holds true:

$$\frac{\varepsilon_{bu}}{\varepsilon_{tu}} \approx 1.6 - 0.099(m-1) + 0.061(m-1)^2 + O\Big((m-1)^3\Big), \quad b = 0. \tag{40}$$

The above simple formula (40) explains the higher tensile strains at the instant of failure that have been found in Laws (1981) from 4PB tests than those from direct tension tests of asbestos cement and a special composite material.

In addition, the ultimate bending moment, M_{bu}, calculated according to failure criterion (38), is always higher than the ultimate moment, M_{tu}, calculated according to the uniaxial stress instability criterion (17), such that the following asymptotic relation is valid:

$$\frac{M_{bu}}{M_{tu}} \approx 1.1456 - 0.0281(m-1) + 0.01675(m-1)^2 + O\Big((m-1)^3\Big), \quad b = 0. \tag{41}$$

The interpretation of the above formula (41) is that structural damage to the beam (measured distortion of the beam as a whole) subjected to bending moment may not occur until the moment reaches a value sufficiently large to cause fracturing not only in the most-stressed outer fiber of the member but in the fibers to a measurable depth of the beam.

As a next step the expression which gives the variation of the bending curvature along the longitudinal axis of the beam (i.e., x axis) is studied based on the stress–strain relations in tension and compression. For this purpose we integrate the second term of Eq. (22), using relationships (7) for $c = 0$, and we derive the following nonlinear constitutive relationship for the bending moment:

$$\hat{M} = \tfrac{1}{3}(\hat{z}_t^3 + m\hat{z}_c^3)\hat{\kappa} + \tfrac{1}{4}(m_f\hat{z}_t^4 - m_b\hat{z}_c^4)\hat{\kappa}^2, \tag{42}$$

where the normalized moment in 3PB configuration is given in terms of the normalized load by the relation,

$$\begin{aligned} &\hat{M} = \frac{\hat{P}}{2}\left(\hat{x} + \frac{L}{2B}\right), \quad 0 \leqslant \hat{x} \leqslant \frac{L}{2B}, \\ &\hat{x} = \frac{x}{B}, \qquad \hat{P} = \frac{P}{E_t H^2}. \end{aligned} \tag{43}$$

Solving Eq. (42) with respect to $\hat{\kappa}$ and employing also relation (43), the following expression for the dimensionless bending curvature is obtained:

$$\hat{\kappa}(\hat{x}) = \frac{1}{3(m_b\hat{z}_c^4 - m_f\hat{z}_t^4)}\left[2(m\hat{z}_c^3 + \hat{z}_t^3) - \sqrt{4(m\hat{z}_c^3 + \hat{z}_t^3)^2 + 18\hat{P}\left(\hat{x} + \frac{L}{2B}\right)(m_f\hat{z}_t^4 - m_b\hat{z}_c^4)}\right]; \quad 0 \leqslant \hat{x} \leqslant \frac{L}{2B}. \tag{44}$$

On the other hand, for the linear elastic material (i.e., $m_f = m_b = 0$), the following simpler expression is derived by solving Eq. (42) with respect to $\hat{\kappa}$:

$$\hat{\kappa}(\hat{x}) = \frac{3}{2}\frac{\hat{P}\left(\hat{x} + \frac{L}{2B}\right)}{[\hat{z}_t^3 + m(1-\hat{z}_t)^3]}, \quad 0 \leqslant \hat{x} \leqslant \frac{L}{2B}. \tag{45}$$

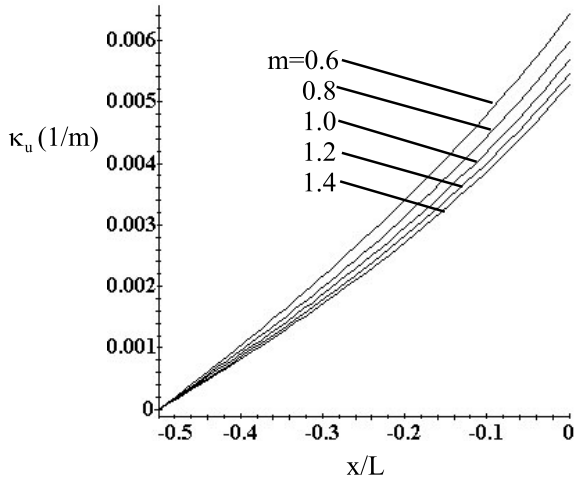

Fig. 7. Variation of bending curvature at failure with distance from centre of beam in the 3PB test for various values of modulus ratio at hand and for $m_f = -1600$.

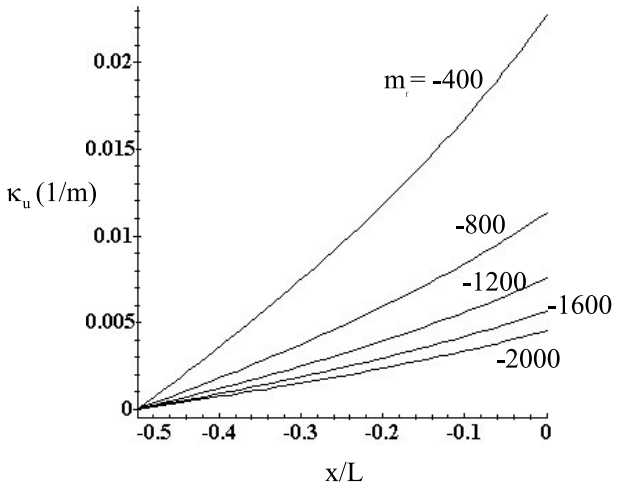

Fig. 8. Distribution of bending curvature at failure along the semi-length of the beam in the 3PB test for various values of damage parameter m_f and for $m = 1$.

Of special interest is the dependence of the ultimate bending curvature at failure denoted herein by the symbol κ_u on the modulus ratio m of the rock and on the damage parameter m_f in the constitutive behavior of the rock in uniaxial tension. Figs. 7 and 8, respectively, illustrate the variation of κ_u along the semi-length of the specimen in 3PB for various values of m at constant m_f, and for various values of m_f at constant m. From these diagrams, it is observed that the ultimate curvature is significantly influenced by m_f, whereas it is slightly affected by the modulus ratio m.

This observation suggests that the damage parameter can be evaluated from measurements of the bending curvature at mid-span of the 3PB specimen at the instant of failure.

3. The local effect of concentrated force in 3PB

The problem of stress distribution in a beam subjected to the action of a concentrated load is of great practical interest and cannot be discarded in the development of a technical theory. At beam sections which are sufficiently far from the central section, in such a way that Saint-Venant's principle is satisfied, the stress distribution is obtained with satisfactory accuracy by the usual Bernoulli–Euler kinematic assumption. Near the point of application of a concentrated force, however, a serious local perturbation in stress distribution should be expected, and therefore the detailed elastic solution is necessary. A similar remark has been made by Love (1927). Also a matter of special interest is the relation of the actual maximum bending stress in 3PB with the respective stress predicted by the Bernoulli–Euler technical theory. This is because the correct relationship between the maximum extensional strain and maximum bending moment in 3PB is of great importance in engineering applications.

In order to illustrate the effect of the localized centrally applied force on the upper straight edge of the beam, or the so-called "punch effect", the distribution of the axial (or longitudinal) and transverse stresses along the height of beam at the central cross-section (also principal stresses since due to symmetry $\tau_{xz} = \tau_{zx} = 0$) were computed numerically by employing the displacement discontinuity technique (DDT) (Crouch and Starfield, 1990). The material model that it was employed was that of a linear elastic (i.e., $m = 1$), isotropic and no-damage material (i.e., $m_f = 0$) and the beam geometry was prescribed by $L = 0.38$ m and $H = 0.10$ m. The distributions of the principal stresses along the height of the beam displayed in Fig. 9 agree qualitatively well with those presented by Coker and Filon (1957), however, it seems that the photoelastic experiments did not capture the abrupt absolute increase of both compressive principal stresses in a thin skin adjacent to the loaded part of the beam. The transverse principal stress σ_{zz} reaches the value of the externally applied stress at the surface of the beam and quickly dies away to a negligible quantity. The symbol $\bar{z}$ in Fig. 9 denotes the distance of the point under consideration from the centroid of the beam.

It can be shown that near to the place of load application and at mid-section the stresses may be approximated well by the solution of uniform normal loading q_0 over a strip of length d of the edge of a half-plane (Muskhelishvili, 1963):

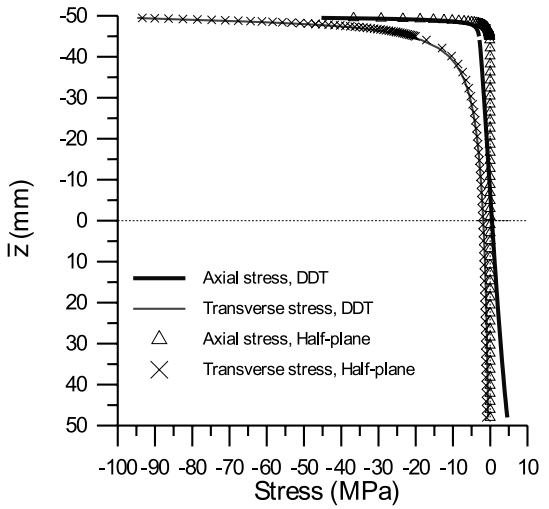

Fig. 9. Plot of vertical distribution of axial and transverse stresses predicted by the DDT model for an applied stress at the upper central region of beam of $q_0 = -100$ MPa that is equivalent to a load $P = 0.008MN$. Compressive stresses are considered to be negative quantities. In the same plot the half-plane solution (46) is also displayed for comparison purposes.

$$\sigma_{xx}^{*}=\frac{q_0}{\pi}\left[\arctan\left[-\frac{(\bar{z}+H/2)}{d},-1\right]+\arctan\left[-\frac{(\bar{z}+H/2)}{d},1\right]+\frac{2(\bar{z}+H/2)d}{(\bar{z}+H/2)^2+d^2}\right],$$
$$\sigma_{zz}^{*}=\frac{q_0}{\pi}\left[\arctan\left[-\frac{(\bar{z}+H/2)}{d},-1\right]+\arctan\left[-\frac{(\bar{z}+H/2)}{d},1\right]-\frac{2(\bar{z}+H/2)d}{(\bar{z}+H/2)^2+d^2}\right], \tag{46}$$

in which $q_0=-100$ MPa, $d=0.8$ mm, $H=0.1$ m for the example under consideration, and the two-argument function $\arctan(y,x)$ computes the principal value of the argument of the complex number $x+\mathrm{i}y$ so that $-\pi<\arctan(y,x)\leqslant\pi$. From the plot of Fig. 9, it may be seen that the transverse stresses that are predicted by the half-plane solution (46) are in very close agreement with the respective stresses deduced by the numerical solution of the DDT model along the whole cross-section. The axial (longitudinal) stresses of the half-plane solution compare well with DDT prediction for very small distances from the upper edge of the beam and then quickly attenuate to reach the zero value.

On the other hand, the axial stress distribution along the central section of the 3PB beam can be calculated by recourse to the following formula due to Timoshenko and Goodier (1970):

$$\sigma_{xx}^{\mathrm{Tim}}=\frac{12P}{BH^3}\left(\frac{L}{4}-\frac{H}{2\pi}\right)\bar{z}+\frac{P}{\pi BH}+\frac{2P}{\pi BH}\left(\frac{4\bar{z}^3}{H^3}-\frac{3\bar{z}}{5H}\right). \tag{47}$$

It is also interesting to observe from Fig. 10 below, which is a detail of the axial stress distribution along the central section shown in Fig. 9, that the neutral axis of the beam is located slightly above the middle axis due to the 'punch effect', which is in agreement with Frocht's photoelasticity results (Frocht, 1957). In Appendix A, it is shown that from the first of relations (46) one may find that the asymptotic value of the parasitic axial force N^* that is produced from the axial stress σ_{xx}^{*} is given by the relation,

$$N^{*}\approx-\frac{2q_0}{\pi}d+\mathrm{O}(d^3). \tag{48}$$

By recourse to the above relationship, as well as the following formula that depicts the tensile outer-fiber distance z_{t} of a linear elastic material in the presence of axial force:

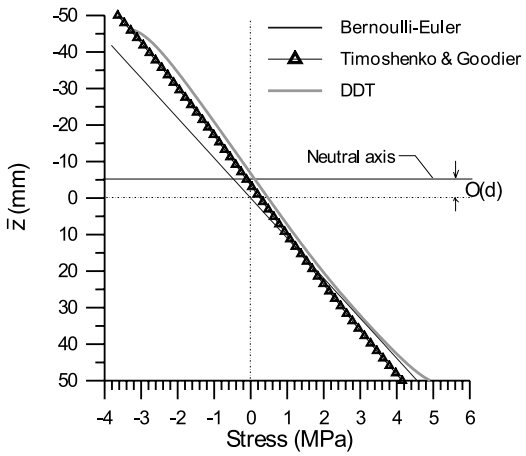

Fig. 10. Detail of the axial stress distribution along central cross-section of the beam obtained from DDT analysis displayed in Fig. 9. The thick line represents the exact solution whereas the line with triangles corrersponds to Timoshenko's solution (47) and the thin line to the linear approximation of elementary beam theory described by the first term of Eq. (50).

$$z_t = \frac{H}{2} + \frac{N^*}{E\kappa H} \approx \frac{H}{2} + \mathrm{O}(d), \tag{49}$$

it is demonstrated that the shift of the neutral axis is of the order of the width d of the strip where the external load is applied. This is also clearly shown in Fig. 10. Furthermore, as can be also observed from Eq. (47) and Fig. 10, the axial stress σ_{xx} does not follow a linear law, whereas at the lower fiber where the maximum tensile stress occurs, its value is higher than would be expected from the elementary beam theory.

Next, based on the above results, we attempt a comparison between the numerical model and the Bernoulli–Euler and Timoshenko's propositions of distribution of axial stresses. It is proved in the mathematical theory of elasticity that in the region of pure bending of a unique modulus or linear material (i.e., $m = 1$) the exact stress state is given by (Frocht, 1957):

$$\sigma_{xx}^{\mathrm{elem}} = \frac{M\bar{z}}{I}, \qquad \sigma_{zz} = 0, \qquad \tau_{xz} = 0. \tag{50}$$

On the other hand, Timoshenko proposes the following more accurate formula that has been derived by Seewald (1927) for the correction of the maximum tensile bending stress in 3PB test configuration by taking into account the geometry of the beam:

$$\beta_{\mathrm{S}} = 1 - 0.177\left(\frac{L}{H}\right)^{-1} \quad \text{at } \bar{z} = H/2, \tag{51}$$

in which

$$\beta_{\mathrm{S}} = \frac{\sigma_{xx}^{\mathrm{S}}}{\sigma_{xx}^{\mathrm{elem}}} \tag{52}$$

with the subscript 'S' denoting Seewald's prediction for the value of axial stress at bottom fiber at mid-section of the beam. On the contrary, based on the numerical DDT linear elastic model the following best-fit formula has been derived for the range of length over height beam ratios $1 \leqslant L/H \leqslant 20$

$$\begin{aligned}\beta_{\mathrm{DDT}} = {} & 1 + 0.76\left(\frac{L}{H}\right)^{-1} - 0.842\left(\frac{L}{H}\right)^{-2} - 3.268\left(\frac{L}{H}\right)^{-3} + 3.24\left(\frac{L}{H}\right)^{-4} \\ & + \mathrm{O}\left[\left(\frac{L}{H}\right)^{-5}\right] \quad \text{at } \bar{z} = H/2, \\ \beta_{\mathrm{DDT}} = {} & \frac{\sigma_{xx}^{\mathrm{DDT}}}{\sigma_{xx}^{\mathrm{elem}}}.\end{aligned} \tag{53}$$

The predictions of the above two correction formulae for the bending stress at the bottom fiber of the beam at its mid-section have been plotted in Fig. 11.

Hence, by using the DDT numerical model, it was demonstrated that Seewald's formula underestimates the maximum tensile stress, probably due to insufficient asymptotic analysis. Timoshenko's less accurate formula predicts that the local effect at the bottom beam edge is equal to $-0.508P/H$, whereas Seewald's more accurate formula (47) gives $-0.266P/H$. However, the predictions of the numerical model show that Bernoulli–Euler formula is very accurate if the depth of the beam is small in comparison with its length. For example for length:depth ratio equal to 14, the error of the Bernoulli–Euler technical theory is less than 5%.

The distribution of axial strains at the central section of the beam is also of special interest both for the prediction of failure load in the former case and for the correction of beam deflections in the latter case. For an isotropic material that exhibits linear elastic behavior, the axial and transverse strains are related to the stresses σ_{xx}, σ_{zz} by the following well known *plane stress* formulae, respectively,

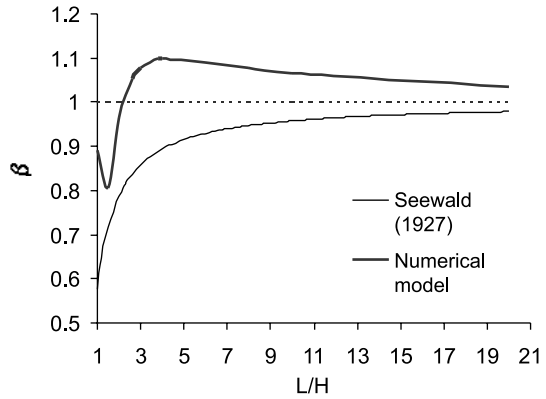

Fig. 11. Comparison of the ratio of maximum bending stresses $\beta_i = \sigma^i_{xx}/\sigma^{\text{elem}}_{xx}$, ($i$ = S, DDT) at bottom edge of the mid-section of the beam in 3PB derived from Seewald's approximate formula and from the DDT numerical solution.

$$\left.\begin{aligned} \varepsilon_{xx} &= \tfrac{1}{E_t}[\sigma_{xx} - \nu\sigma_{zz}], \\ \varepsilon_{zz} &= \tfrac{1}{E_t}[\sigma_{zz} - \nu\sigma_{xx}] \end{aligned}\right\}, \tag{54a}$$

From the above relation (54a), it may be seen that if $\nu\sigma_{zz} > \sigma_{xx}$ in the upper part of the face of the beam then an extensional axial strain will occur since both stresses are compressive in that region.

A plot displaying the distribution of normalized axial strains ($E_t\varepsilon_{xx}$) corresponding to various Poisson's ratios of a linear elastic rock material and calculated by using the first relation (54a) for the model example presented above is shown in Fig. 12. From the figure, it is noted that for values of Poisson's ratio above 0.25

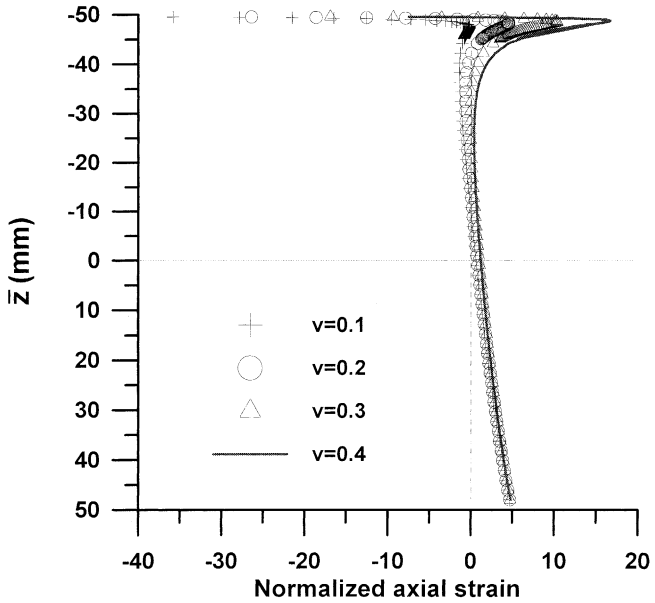

Fig. 12. Distribution of axial strain along the height of the beam of $L/H = 3.8$ and for $P = 0.008MN$ at mid-span for four values of Poisson's ratio at hand.

the axial strain at mid-span is tensile almost along the entire height of the beam. On the other hand, it may be shown that the tranverse strains ε_{zz} along the height of the beam are always compressive. Therefore, the moduli of elasticity in tension and compression may be derived from back analysis of measured axial and transverse strain measurements at mid-section of the 3PB beam assuming that the stresses are given by the isotropic theory. In this case, the following bilinear formulae may be applied for the computation of strains that match better the experimental results:

$$\left.\begin{aligned}\varepsilon_{xx} &= \tfrac{1}{E_t}\left[\sigma_{xx} - \tfrac{v_c}{m}\sigma_{zz}\right],\\ \varepsilon_{zz} &= \tfrac{1}{E_c}\left[\sigma_{zz} - v_t m\sigma_{xx}\right]\end{aligned}\right\}, \tag{54b}$$

where v_t, v_c are the Poisson's ratios in uniaxial tension and compression, respectively.

Another remark of practical importance that can be inferred from Fig. 12 is that for most types of rocks which are characterized by Poisson's ratios in the range 0.25–0.35, Gerstner's $(d\sigma/d\varepsilon)$ failure criterion is possibly valid in the 3PB configuration. In other words, the maximum tensile strain in bending should coincide with that in uniaxial tension. This is because for this range of Poisson's ratio the central cross-section of the beam is under extension almost along its full length. This remark is in contradiction with the much higher failure strain predicted by the $(dM/d\varepsilon)$ failure criterion proposed by Bert and Kumar (1980) (for example see relation (40)). As it is demonstrated in Part II of this work, the only way to investigate the applicability of these two failure criteria is by means of appropriate experiments.

4. Prediction of failure load and modulus of rupture of nonlinear rocks exhibiting different behavior in tension and compression

Next, we proceed to the estimation of the critical bending failure loads in 3PB which are predicted by the present *nonlinear* and *Bernoulli–Euler* linear technical theories, respectively. Solving Eq. (42) for load $\hat{P}$ at mid-span (i.e., $\hat{x} = 0$) based on relation (43), substituting the value of the normalized bending curvature $\hat{\kappa} = \varepsilon_f/\hat{z}_t$ and further assuming that $m_b \to 0$, it is obtained

$$P_f = \frac{48E_tI}{LH}\left\{\frac{1}{3}\left[\hat{z}_t^2 + \frac{m}{\hat{z}_t}(1-\hat{z}_t)^3\right] + \frac{1}{4}(m_f\varepsilon_f)\hat{z}_t^2\right\}\varepsilon_f, \quad m_b = 0; \qquad \hat{x} = 0, \tag{55}$$

where P_f denotes the failure load in 3PB and ε_f the maximum extension strain at failure. In the first place, we would like to derive a formula for the ratio of failure load predicted by the nonlinear-bimodular material model over the failure load predicted by a linear, unique-modulus material model. It can be shown that the failure load P_f^* in the framework of the linear theory ($m = 1$) is given by the relationship,

$$P_f^* = \frac{8E_tI}{LH}\varepsilon_f, \quad m = 1. \tag{56}$$

In a conservative beam design ε_f could be taken equal to the value of critical strain ε_{tu} obtained from Gerstner's failure criterion in pure tension. By observing from the first term of relationship (18) that the present material model predicts at failure $D_f = -m_f\varepsilon_f = 1/2$, then by dividing by parts relationship (55) with (56), the following dimensionless failure load is obtained:

$$\lambda^* = \frac{P_f}{P_f^*} = \left\{2\left[1 + m\left(\frac{1}{\hat{z}_t} - 1\right)^3\right] - \frac{3}{4}\right\}\hat{z}_t^2, \quad m_b = 0. \tag{57}$$

Finally, by substituting into Eq. (57), the value of the dimensionless tensile outermost distance $\hat{z}_t$ as it given by the first term of Eq. (28), it is derived

$$\lambda^* = \frac{\frac{5}{4} + \frac{4}{3}\sqrt{\frac{2}{3m}}}{\left(1 + \sqrt{\frac{2}{3m}}\right)^2}, \quad m_b = 0. \tag{58}$$

For the case of $m = 1$ or $E_c = E_t$, the above formula predicts

$$\lambda^* = \frac{1}{4}\left(11 - 10\sqrt{\frac{2}{3}}\right) \approx 0.709, \tag{59}$$

i.e., the linear technical bending theory overestimates the failure load approximately by 41% with respect to the maximum load that can be endured by a nonlinear rock exhibiting damage.

From Eq. (58), it can be found that the limit of the dimensionless failure load as the modulus ratio m approaches the zero value, is zero, i.e.,

$$\lim_{m\to 0} \lambda^* = 0, \tag{60}$$

whereas the respective limit as the modulus ratio tends to infinity

$$\lim_{m\to\infty} \lambda^* = \frac{5}{4}. \tag{61}$$

Fig. 13 presents the dependence of the dimensionless failure load in 3PB on the tangent modulus ratio that is depicted by relation (58) for a material that obeys a parabolic law in pure tension and linear law in unconfined compression. In the same plot the asymptotic value of the failure load for $m \to \infty$ or $E_t \to 0$, as

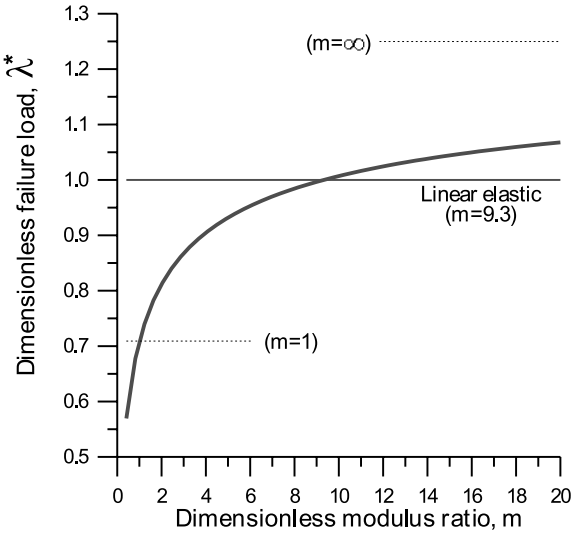

Fig. 13. Plot of dimensionless failure load $\lambda^* = P_f/P_f^*$ in 3PB versus the dimensionless modulus ratio $m = E_c/E_t$.

well as the value for the unique-modulus-nonlinear material is illustrated with dashed lines. Note that the linear elastic case ($\lambda^* = 1$) corresponds here to a modulus ratio of

$$m = \frac{24}{81}(17 + 4\sqrt{13}) \approx 9.310. \tag{62}$$

The important conclusion that is drawn from the above diagram is that the "actual" failure load predicted by the proposed nonlinear theory is always lower than that predicted by linear, unique-modulus theory for $0 \leqslant m \leqslant 9$. Since rocks frequently exhibit double elasticity (Table 1) and nonlinearity due to damage evolution, failure to evaluate the possible differences between the compressive and tensile elastic properties, as well as nonlinearity of rock manifested in the uniaxial tensile regime can severely affect design validity. Finally, the following relation may be found for the dimensionless failure load as a function of ratio m and ultimate value of the damage D_f:

$$\lambda^* = \frac{2 - \frac{3}{2}D_f + \frac{2}{\sqrt{m}}\sqrt[3]{1 - \frac{2}{3}D_f}}{\left(1 + \sqrt{\frac{1}{m} - \frac{2D_f}{3m}}\right)^2}, \quad m_b = 0. \tag{63}$$

Next, the "modulus of rupture" defined as the tensile stress in the outer fiber at failure and calculated by beam theory, is frequently used in place of the tensile strength because of the difficulty of direct tensile testing (Obert and Duvall, 1967). The equation that gives the modulus of rupture is

$$\sigma_{bu} = \beta\frac{M\bar{z}}{I}, \quad \bar{z} = \frac{H}{2}, \tag{64}$$

where σ_{bu} denotes the modulus of rupture and β, the correction term in case of punch effect in 3PB treated in Section 3. It is to be emphasized that the value obtained by use of Eq. (64) which neglects the double elasticity of materials is *not* a true strength value; it is just an index of moment-carrying ability expressed in units of force per unit area. It is worth noticing that the clear disagreement of the values of the ultimate tensile stress in bending and in tension was first observed in the testing of concrete. More than a half a century ago, Gonnerman and Shuman (1928) published results of tests indicating very conclusively that the maximum tensile stress in concrete at rupture in pure tension and pure bending are not even close. Jaeger and Hoskins (1966), on the other hand, have compared the values of the direct uniaxial tensile strength of three different rocks with values obtained from 3PB tests. These values are displayed in Table 2. It may be seen from the table that the tensile strength values obtained from the 3PB tests – that involve non-uniform stress distribution – are almost twice as great of the values referring to the direct tension tests. Experimental results of Brooks and Neville (1977) referring to the variation of ratio of bending to direct tension strength with the tensile strength of dry concrete are displayed in Fig. 14.

The above experimental results presented in Fig. 14 and Table 2 clearly demonstrate that neglecting the properties of the rock in uniaxial tension, as it happens customarily in current mining and rock engineering

Table 2
Comparison of tensile strengths of three rock types measured from direct and indirect tensile tests (Jaeger and Hoskins, 1966)

Rock	σ_{cu}/σ_{tu}	Uniaxial tensile strength (MPa)	3PB strength (MPa)	Tensile strength ratio
Carrara marble	13	6.9	11.8	1.71
Gosford sandstone	13.5	3.6	7.9	2.19
Bowral trachyte	10.9	13.7	25.2	1.84

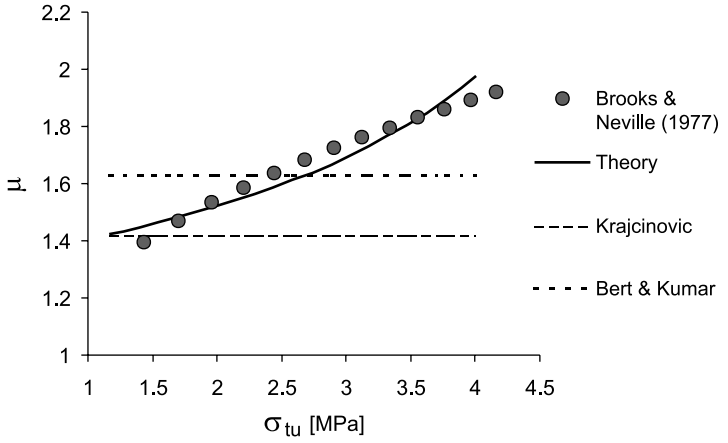

Fig. 14. Experimental results pertaining to the variation of tensile strength ration μ on the uniaxial tension strength of dry concrete (Brooks and Neville, 1977). The predictions of the proposed nonlinear theory and of Krajcinovic (1979) and Bert and Kumar (1980) are displayed in the same figure.

design practice, is not only wrong, but also it may result in significant errors in evaluating the true tensile strength properties of rocks from a bending test.

According to Gerstner's $(\mathrm{d}\sigma/\mathrm{d}\varepsilon)$-failure criterion for uniform axial tension leads to the first term of expression (20) for σ_{tu}. Thus, by putting $M = P_{\mathrm{f}}L/4$ into relationship (64) for the 3PB configuration, substituting the value of the failure load P_{f} as it given by relation (55) and dividing with the value of σ_{tu} given by the first term of relation (20), we deduce

$$\mu = \frac{\sigma_{\mathrm{bu}}}{\sigma_{\mathrm{tu}}} = \frac{\beta}{(1-D_{\mathrm{f}})}\left[\frac{\frac{5}{4}+\frac{4}{3}\sqrt{\frac{2}{3m}}}{\left(1+\sqrt{\frac{2}{3m}}\right)^2}\right], \quad m_{\mathrm{b}} = 0. \tag{65}$$

In Fig. 15, the variation of the relative moduli of rupture on the modulus ratio computed by virtue of Eq. (65) and for $D_{\mathrm{f}} = 0.5$ (i.e., Gerstner's failure criterion) is graphically displayed.

For the specific case of linear material ($m = 1$) and for $\beta = 1$, $D_{\mathrm{f}} = 0.5$ (i.e., for the infinitely long beam) the above formula (65) gives

$$\mu = \frac{1}{2}\left(11 - 10\sqrt{\frac{2}{3}}\right) = 1.42, \quad m = 1. \tag{66}$$

The above value of the strength ratio agrees with the value deduced by Krajcinovic (1979) who also employed the $(\mathrm{d}\sigma/\mathrm{d}\varepsilon)$-failure criterion. It is worth noting that the difference in the relative modulus of rupture in pure bending and pure tension is fully recognized by the ACI Code for concrete. According to ACI Standard 318-71 (1970)

$$\mu = 1.5. \tag{67}$$

It is mentioned here that the special technical committee of the European Committee for Standardization (CEN) CEN/TC 246 for "Natural Stone Test Methods" does not consider the aforementioned difference in bending and uniaxial tension that is exhibited by natural stone materials. It can be easily seen

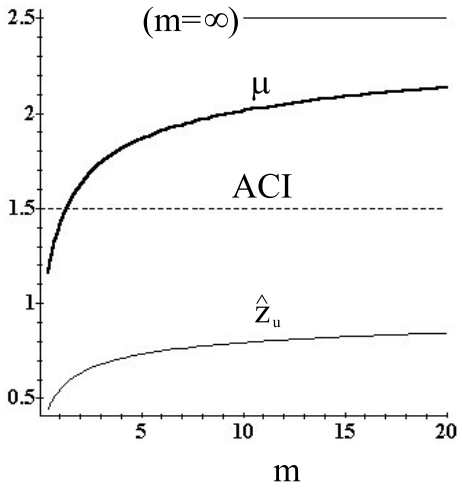

Fig. 15. Dependence of tensile stress ratio on the elasticity modulus ratio computed by relationship (65) for $\beta = 1$ and $D_f = 0.5$. In the same plot, the variation of the outermost tensile distance at failure on the modulus ratio is also illustrated.

that the limit values of the relative modulus of rupture given by relationship (65) for $D_f = 0.5$, $m \to 0$ and $m \to \infty$ (no-tension material), respectively, are given by the formulae,

$$\lim_{m\to 0}\mu = 0, \qquad \lim_{m\to\infty}\mu = 2.5\beta. \tag{68}$$

Finally, Bert and Kumar (1980) by using a failure criterion of the type $dM/d\varepsilon$ have found the following tensile strength ratio in the case of single-modulus material (i.e., $m = 1$)

$$\mu = 1.63. \tag{69}$$

Finally, by recourse to the proposed theory it is demonstrated in Fig. 14 and Appendix B (the data presented at Table 3 have been used in Fig. 14) that the experimental data of Brooks and Neville (1977) may be predicted very well for $m = 1$ and $m_b < 0$, i.e., by considering that the concrete exhibits damage in

Table 3
Model predictions pertaining to the dependence of the strain ratio $\bar{\varepsilon}$, position of neutral axis $\hat{z}_t$ and strength ratio μ on the value of damage parameter D_c in compression. The last column are the experimental tensile strength of concrete specimens (Brooks and Neville, 1977)

D_c	$\bar{\varepsilon}$	$\hat{z}_t$	μ	σ_{tu} (MPa)
−0.01	0.81873	0.54983	1.42353	1.16146
−0.05	0.828	0.54705	1.44876	1.39859
−0.1	0.84038	0.54337	1.48322	1.695
−0.15	0.85375	0.53945	1.52144	1.99141
−0.2	0.86831	0.53524	1.56414	2.28781
−0.25	0.88425	0.53071	1.61224	2.58422
−0.3	0.90188	0.5258	1.66698	2.88063
−0.35	0.92157	0.52041	1.73005	3.17704
−0.4	0.94388	0.51443	1.80384	3.47344
−0.45	0.96961	0.50772	1.89193	3.76985
−0.49	0.99346	0.50164	1.9764	4.00698

compression regime as well. It should be mentioned that the predictions proposed by Krajcinovic (1979) and Bert and Kumar (1980) for the same set of data are given by relations (66) and (69), respectively.

5. Concluding remarks

A technical beam theory based on Bernoulli–Euler kinematic assumption was developed for rocks exhibiting a polynomial nonlinear stress–strain behavior that is different in the tensile and compressive regimes. Distinction is made between two types of nonlinearity, namely:

- one that occurs in the small strain regime and corresponds to the transition region between the tension and compression linear portions of the stress–strain curve – herein referred as "double elasticity" and may be realized as a special type of anisotropy – and
- another that occurs at sufficient large strains due to damage of the material manifested by initiation and propagation of cracks in the tensile regime, or due to consolidation of porous material in the initial stages of compressive loading.

Since the correct relation between the maximum extensional strain and maximum bending moment in flexure is of great importance in engineering applications, we propose a correction for the maximum bending stress at the central section of a beam subjected centrally to the action of a concentrated load. Further, it is shown that above some value of Poisson's ratio the central section of a beam in 3PB is under extension almost along its full length, therefore Gerstner's $(d\sigma/d\varepsilon)$ failure criterion should be applied in this testing configuration rather than the $(dM/d\varepsilon)$ criterion that predicts higher ultimate bending stress. It is also shown that the lengthwise distribution of bending curvature is nonlinear with a peak value at mid-span for the case of 3PB; this peak value of the bending curvature depends both on modulus ratio m and damage parameter m_f in the tensile regime and formulae are displayed for the computation of the damage parameter from measurements of bending curvature at the central section of the beam for known modulus ratio m.

Since rock frequently displays double elasticity and damage, failure to evaluate the possible differences between the compressive and the tensile elastic properties, as well as the nonlinearity in the uniaxial tension regime can severely affect design validity. Yet this is what has frequently occurred in rock mechanics, where due to the inherent difficulties of direct tensile testing, the tensile modulus of elasticity is often assumed to be equal to the compressive value (i.e., it is assumed that $m = 1$). An important conclusion that is drawn from this work is that the actual failure load predicted by the double elasticity-nonlinear theory is always lower than that predicted by the linear theory for $0 \leqslant m \leqslant 9.3$.

Further, it is illustrated that the bimodularity of quasi-brittle materials may result in the variation of the ratio of modulus of rupture over the tensile strength in the range of 0–2.5. Thus, failure to evaluate properly the possible differences between the compressive and tensile elasticity of rocks, as well as nonlinearity of rocks in the uniaxial tensile regime can severely affect the design validity.

Finally, it is demonstrated that the consideration of nonlinearity of concrete in both the compression and tension regimes leads to an expression for the ratio of modulus of rupture over the tensile strength as a function of the tensile strength that is in accordance with published experimental data.

Acknowledgements

The authors gratefully acknowledge the financial support of the European Union DG XII, SMT Programme under the contract SMT4-CT96-2130. Further, the authors acknowledge the remarks that were made by the anonymous reviewers.

Appendix A

The axial force N^* that is produced by the axial stress σ^*_{xx} may be found as follows:

$$N^* = \int_0^H \sigma^*_{xx}\,\mathrm{d}z^*, \tag{A.1}$$

where we have set the dimensionless variable,

$$z^* = \frac{\overline{z} + \frac{H}{2}}{d}. \tag{A.2}$$

By inserting into Eq. (A.1) the value of the axial stress as it given by the first term of Eq. (46) and performing an asymptotic analysis for very small values of d, we obtain

$$N^* \approx -\frac{2q_0}{\pi} d + \mathrm{O}\left(d^3\right). \tag{A.3}$$

Also the bending moment M^* generated by σ^*_{xx} may be found from Eq. (A.3) to be

$$M^* = N^* \frac{H}{2} \approx \mathrm{O}(d) q_0. \tag{A.4}$$

The position of the neutral axis of the linear elastic beam characterized by a modulus of elasticity E, may be obtained from the first term of equilibrium relation (34) by putting in the right-hand side the axial force that is produced by the concentrated load

$$\int_{-z_\mathrm{c}}^{0} E\varepsilon_\mathrm{c}\,\mathrm{d}z + \int_0^{z_\mathrm{t}} E\varepsilon_\mathrm{t}\,\mathrm{d}z = N^*. \tag{A.5}$$

Finally, by substituting in the left-hand side of Eq. (A.5), the approximate expression of N^* as it given by Eq. (A.3), putting $z_\mathrm{c} = H - z_\mathrm{t}$, and solving for the value of the tensile outer fiber distance z_t, we deduce

$$z_\mathrm{t} \approx \frac{H}{2} + \mathrm{O}(d). \tag{A.6}$$

Appendix B

The maximum compressive strain may be found from the equilibrium of axial forces described by Eq. (24)

$$\int_0^{\varepsilon_\mathrm{c}} \sigma_\mathrm{c}(\varepsilon)\,\mathrm{d}\varepsilon = \int_0^{\varepsilon_\mathrm{t}} \sigma_\mathrm{t}(\varepsilon)\,\mathrm{d}\varepsilon \iff \int_{-\varepsilon_\mathrm{c}}^{\varepsilon_\mathrm{t}} \sigma(\varepsilon)\,\mathrm{d}\varepsilon = 0. \tag{B.1}$$

Application of constitutive equations (7) into Eq. (B.1) and making the necessary integrations and algebraic manipulations the following equation is derived:

$$\varepsilon_\mathrm{c}^3 + \frac{3m}{2m_\mathrm{b}}\varepsilon_\mathrm{c}^2 - \left[\frac{3}{2m_\mathrm{b}} + \frac{m_\mathrm{f}}{m_\mathrm{b}}\varepsilon_\mathrm{t}\right]\varepsilon_\mathrm{t}^2 = 0, \tag{B.2}$$

where we have employed the non-dimensional variables as they are defined by Eq. (26). The above cubic Eq. (B.2) may be put into the form:

$$D_c\bar{\varepsilon}^3+\frac{3}{2}m\bar{\varepsilon}^2-\left(\frac{3}{2}-D_t\right)=0,$$
$$D_c=m_b\varepsilon_t,\qquad \bar{\varepsilon}=\frac{\varepsilon_c}{\varepsilon_t},\qquad D_t=-m_f\varepsilon_t. \tag{B.3}$$

If $D_c<0$ (or $m_b<0$ since all strain quantities are considered positive) then the material exhibits damage, whereas in the opposite case (i.e., $D_c>0$) the material exhibits stiffening, upon compressive loading. The discriminant of the above cubic equation is

$$\mathrm{Dis}=\frac{27}{4}(3-2D_t)\left(2D_c^2D_t-3D_c^2+m^3\right). \tag{B.4}$$

The cubic equation (B.3) possesses three real roots (with two of them equal) provided that its discriminant (B.4) is positive. The two equal roots that are also the answer to our problem are given by the relation,

$$\bar{\varepsilon}=-\frac{1}{4D_c}\left(q+\frac{m^2}{q}+2m\right),$$
$$q=\sqrt[3]{6D_c^2-4D_c^2D_t-m^3+2D_c\sqrt{9D_c^2-12D_c^2D_t-3m^3+4D_c^2D_t^2+2D_tm^3}}. \tag{B.5}$$

In order to check the validity of the proposed model to predict the experimental results of Brooks and Neville (1977), we have estimated the value of strain ratio $\bar{\varepsilon}$ based on (B.5), and on the ultimate value of $D_t=0.5$ for $m=1$ and for D_c ranging from –0.01 to –0.49. Then we have assumed a one-to-one correspondence of the damage parameter in the compression regime, D_c, with the ultimate tensile strength of concrete specimens as it is illustrated in Table 3. The values of the position of the neutral axis and of the bending strength ratio have been subsequently calculated by recourse to the methodology proposed in Sections 2.3 and 2.4 respectively, i.e.,

$$\hat{z}_t=\frac{1}{1+\bar{\varepsilon}},$$
$$\mu=6\frac{[m(1-\hat{z}_t^2)-\hat{z}_t^2][\hat{z}_t^3+m(1-\hat{z}_t)^3]}{-D_t\hat{z}_t^3+D_c(1-\hat{z}_t)^3}-\frac{27}{4}\frac{[D_t\hat{z}_t^4+D_c(1-\hat{z}_t)^4][m(1-\hat{z}_t)^2-\hat{z}_t^2]^2}{[-D_t\hat{z}_t^3+D_c(1-\hat{z}_t)^3]^2}. \tag{B.6}$$

References

Adler, L., 1970. Evaluating double elasticity in drill cores under flexure. Int. J. Rock Mech. Min. Sci. 7, 357–370.

Bach, C., Baumann, R., 1914. Elastizitat und Festigkeit, Ninth ed., Springer, Berlin, p. 259.

Barla, G., Goffi, L., 1974. Direct tensile testing of anisotropic rocks. Proc. Third Int. Congr. Rock Mechanics, vol. 2. Part A, Denver, 93–98.

Bell, J.F., 1984. Encyclopedia of Physics. In: Truesdell, C., Mechanics of Solids, vol. I. Springer, Berlin.

Bert, C.W., Kumar, M., 1980. J. Appl. Mech. 47, 449–450.

Bert, C.W., 1983. Prediction of bending rupture strength of non-linear materials with different behavior in tension and compression. Int. J. Non-Linear Mech. 18 (5), 353–361.

Blair, B.E., 1956. Physical properties of mine rock. Part IV. U.S. Bureau of Mines Research and Investigation, 5244, pp. 12, 16, 35, 50.

Brace, W.F., 1965. Some new measurements of linear compressibility of rocks. J. Geophys. Res. 70 (2), 391–398.

Brooks, J.J., Neville, A.M., 1977. A comparison of creep, elasticity and strength of concrete in tension and in compression. Mag. Concr. Res. 29, 131–141.

Building Code Requirements for Reinforced Concrete (ACI Standard 318-71), 1970. American Concrete Institute, P.O. Box 4754, Redford Station, Mich.

Clark, S.K., 1963. The plane elastic characteristics of cord-rubber laminates. Text. Res. J. 33, 295–313.

Coker, E.G., Filon, L.N.G., 1957. A Treatise on Photo-elasticity. University Press, Cambridge.
Crouch, S.L., Starfield, A.M., 1990. Boundary Element Methods in Solid Mechanics. Unwin Hyman, London.
Engesser, F., 1895. Schweiz. Bauz. 26.
Exadaktylos, G.E., Vardoulakis, I., Kourkoulis, S.K., 2000. Influence of nonlinearity and double elasticity on flexure of rock beams-II. Characterization of Dionysos marble, submitted for publication.
Fairhurst, C., 1961. Laboratory measurement of some physical properties of rock. Proc. Fourth Symp. Rock Mechanics Bull. 76, Mineral and Experiment Station, Pennsylvania State Univ. Park, 105–118.
Frocht, M.M., 1957. Photoelasticity, vol. I. Wiley, New York.
Gilbert, G.N.J., 1961. Stress/strain properties of cast iron and Poisson's ratio in tension and compression. B. C. I. R. Jl 9, 347–363.
Gonnerman, H., Shuman, E.C., 1928. Compression flexure and tension tests of plain concrete. Proceedings ASTM 28 (Part 2), 527–573.
Haimson, B.C., Tharp, T.M., 1974. Stresses around boreholes in bilinear elastic rock. Soc. Petroleum Engrs J. 14, 145–151.
Hartig, E., 1893. Der Elastizitatmodul der geraden Stabes als Funktion der Spezifischen Beanspruchung. Civilingenieur B. XXXIX, 113–138.
Jaeger, J.C., Cook, N.G.W., 1976. Fundamentals of Rock Mechanics, second ed. Chapman and Hall, London.
Jaeger, J.C., Hoskins, E.R., 1966. Stresses and failure in rings of rock loaded in diametral tension or compression. Br. J. Appl. Phys. 17, 685–692.
Janson, J., Hult, J., 1977. Fracture mechanics and damage mechanics, a combined approach. J. Mech. Appl. 1, 69–84.
Korres, M., 1993. From Pendeli to Parthenon. Melissa, Athens, Greece.
Krajcinovic, D., 1979. Distributed damage theory of beams in pure bending. J. Appl. Mech. 46, 592–596.
Laws, V., 1981. Derivation of the tensile stress–strain curve from bending data. J. Mater. Sci. 16, 1299–1304.
Love, A.E.H., 1927. A treatise on the mathematical theory of elasticity, Fourth ed., University Press, London.
Marin, J., 1962. Mechanical Behavior of Engineering Materials. Prentice-Hall, London.
Muskhelishvili, N.I., 1963. Some Basic Problems of the Mathematical Theory of Elasticity. P. Noordhoff, Groningen, The Netherlands.
Nadai, A., 1950. Theory of Flow and Fracture of Solids, vol. 1, Second ed. McGraw-Hill, New York.
Nova, R., Zaninetti, A., 1990. An investigation into the tensile behavior of a schistose rock. Int. J. Rock Mech. Min. Sci. Geomech. Abstr. 27, 231–242.
Obert, L., Duvall, W.I., 1967. Rock Mechanics and the Design of Structures in Rock. Wiley, New York.
Pearsall, G.W., Roberts, V.L., 1978. Passive mechanical properties of aterine muscle myometrium. J. Biomech. 11, 167–176.
Saint-Venant, B., 1864. Notes to the third edition of Navier's Resume des lecons de la resistance des corsps solides, Paris, p. 175.
Seefried, K.J., Gesund, H., Pincus, G., 1967. An experimental investigation of the strain distribution in the split cylinder test. J. Mater. 2, 703–718.
Seewald, F., 1927. Abhandl. Aerodynam. Inst., Tech. Hochschule Aachen 7.
Simkin, A., Robin, G., 1973. The mechanical testing of bone in bending. J. Biomech. 6, 31–39.
Timoshenko, S., 1956. Strength of Materials. Part II: Advanced Theory and Problems, Third ed. Van Nostrand Reinhold, NY.
Timoshenko, S.P., Goodier, J.N., 1970. Theory of Elasticity, Third ed. McGraw-Hill, New York.
Walsh, J.B., Brace, W.F., 1966. Elasticity of rock: a review of some recent theoretical studies. Rock Mech. Engng. Geol. 4 (4), 283–297.
Walsh, J.B., 1965. The effect of cracks on the uniaxial elastic compression of rocks. J. Geophys. Res. 70 (2), 399–411.
Wuerker, R.G., 1955. Measuring the tensile strength of rocks. Trans. AIME 202, 157.
Zambas, C., 1994. Mechanical Properties of Pentelic marbles. Committee for the Restoration of Parthenon Publications, Athens.
Zemlyakov, I.P., 1965. On the difference in the moduli of elasticity of polyamides subjected to different kinds of deformation. Polym. Mech. 1, 25–27.